Key Engineering Materials
ISSN: 1662-9795, Vol. 840, pp 71-78
doi:10.4028/www.scientific.net/KEM.840.71

Submitted: 2019-06-26
Revised: 2019-11-11
Accepted: 2019-11-11
Online: 2020-04-24

$Ni_{0.5}V_{0.5}Fe_2O_4$ Nanophotocatalyst: Preparation, Characterization and its Activity on Remazol Golden Yellow Degradation under Sunlight Irradiation

Rudy Situmeang[1,a*], Romiyati Romiyati[1,b], Ahmad Ammar Saputra[1,c] and Simon Sembiring[2,d]

[1]Department of Chemistry, University of Lampung, Bandar Lampung 35145, Indonesia

[2]Department of Physics, University of Lampung, Bandar Lampung 35145, Indonesia

[a]rudy.tahan@fmipa.unila.ac.id, [b]romiyati0911@yahoo.co.id, [c]ahmadammarssaputra@gmail.com, [d]simon.sembiring@fmipa.unila.ac.id

Keywords: Nano spinel, photodegradation, sol-gel, sunlight irradiation, dye

Abstract. Photocatalysis is a promising solution for the degradation of dyes since this substance give a negative impact on the environment. In this study, $Ni_{0.5}V_{0.5}Fe_2O_4$ nanophotocatalyst was prepared simultaneously using sol-gel and freeze-drying methods. After the freeze-drying process, the sample was subjected to calcination treatment and subsequently characterized using the techniques of X-ray Diffraction (XRD) and Scherrer calculation method, FTIR, DR spectroscopy, and TEM analysis. The results of XRD characterization indicated that material consists of $Ni_{0.5}V_{0.5}Fe_2O_4$ spinel as a major crystalline phase. Then, TEM analysis proved that the grain size of this spinel is in the range of 20 nm. Crystallite size calculation using Scherrer equation proved that the size is 34.06 nm, DRS analysis indicated that bandgap energy of spinel $Ni_{0.5}V_{0.5}Fe_2O_4$ is suitably utilized and FTIR spectra analysis implied that the prominent acid sites are Lewis acid. Furthermore, results of dyes photodegradation indicated that $Ni_{0.5}V_{0.5}Fe_2O_4$ nanocatalyst is active for remazol golden yellow degradation until 45% conversion under sunlight irradiation for 100 min.

Introduction

Remazol golden yellow is one of the dyes that is extensively used in the small and large textile industry. The use of these dyes is due to their bright and shining color so that the appearance of textiles becomes attractive. Because most of the dye during the coloring process is in the solution, wastewater contains a lot of these dyes. So that if the wastewater is channeled into water bodies such as gutters, creeks, rivers, and lakes, it will cause pollution that affects the biota system and ultimately disturb human health. To prevent its effect, the removal of dyes from wastewater must be carried out using scientific methods such as biological, physical and chemical methods [1]. One of the promising chemical methods is photocatalysis.

In photocatalysis, for example, materials that are applied to degrade dyes in wastewater are TiO_2 which was able to remove remazol brown dye as much as 20% [2] and was also able to degrade the commercial azo dyes as much as 11% [3]. Another material that was used to degrade remazol golden yellow as much as 63% is perovskite of $NaNbO_3$ [4].

In terms of spinel compounds, this substance has attracted a lot of attention because its properties are suitable for various applications, such as optical coating or host matrix [5, 6], high-temperature ceramic materials [7, 8], electronic devices [9, 10], magnetic materials [11, 12], pigments [13, 14], and photocatalysis [15, 16]. In principle, the applications of these spinel compounds are governed by peculiar properties that depend on the chemical composition and microstructure of the compound.

A kind of important spinel nanoferrite, as an example, is $NiFe_2O_4$ which has attracted much interest because of its fascinating magnetic and electromagnetic properties [17], catalytic manners [18,19], magnetic characteristics [20, 21], and conducting properties [22]. $NiFe_2O_4$ is a cubic ferromagnetic oxide with a typical normal or inverse spinel structure where Ni^{2+} ions occupy octahedral B-sites and Fe^{3+} ions equally or nonstoichiometric distributed between tetrahedral A-sites and octahedral B-sites [23]. In general, nanosize $NiFe_2O_4$ ferrites have been successfully synthesized by various methods

including sol-gel [24, 25], co-precipitation [26, 27], and other reaction methods, such as reverse micelle [28], thermal plasma [29], and chelating agent [30].

In addition to this study, ferrite nickel spinel is doped by vanadium because vanadium can increase photocatalytic activity as shown by V/TiO_2 catalyst oxidizes ethanol [31] and vanadium catalyst doped on $g\text{-}C_3N_4/TiO_2$ on the antibacterial activity [32] and vanadium oxide supported on porous TiO_2 for phenol photodegradation [33]. Although photocatalysis can use various sources of energy such as visible light, violet light, infrared and x-ray, in this study sunlight irradiation is chosen because the catalyst can work directly in a polluted environment.

So that in this chance, we report the preparation and characterization of spinel multi-components, $Ni_{0.5}V_{0.5}Fe_2O_4$, using simultaneous sol-gel and freeze-drying methods to directly synthesize a uniform, nanostructured $Ni_{0.5}V_{0.5}Fe_2O_4$. In addition, the acid sites properties, crystalline phases, morphology and grain size of final products, band-gap energy value, and catalytic activity have been observed and reported here.

Experimental Section

Materials. Materials used in this work are pectin powder, $Ni(NO_3)_2.6H_2O$ (Merck, 99%), $Fe(NO_3)_3.9H_2O$ (Merck, 99%), NH_4VO_3 (Merck, 99%), pyridine (C_5H_5N, J.T Baker), NH_3 (Merck, 99%), remazol golden yellow and pectin (domestic market), and distilled water.

Instrumentations. The instruments used for characterization were Fourier Transform Infrared (FTIR) spectrometer (Shimadzu Prestige-21) for identifying the presence of functional groups, a Philips X-ray Diffractometer (XRD) model PW 1710 with Cu-Kα radiation for structural identification, Diffuse Reflectance UV-Vis Spectroscopy (Agilent Cary 60) for measuring band-gap energy and Transmission Electron Microscopy (TEM) for identifying grain size distribution and crystallite morphology.

Preparation of $Ni_{0.5}V_{0.5}Fe_2O_4$. A stoichiometric amount of Ni (II) nitrate hydrates, ammonium vanadates, and Fe (III) nitrate hydrates were dissolved in distilled water, having compositions $Ni_{0.5}V_{0.5}Fe_2O_4$ under magnetic stirring for 1 h, respectively, followed by mixing each solution to make final solution weight ratio between nitrates to pectin is 3:2. Adjust the pH=11 in the above solution by addition of ammonia, and heat it at 80 °C with continuous stirring to form a viscous gel. Dried the gel using freeze dryer for 7 h to form the precursors' networks and calcined at 600 °C for 3 h. Finally, V doped Ni-ferrite nano photocatalyst as prepared.

Characterization of $Ni_{1-x}V_xFe_2O_4$

X-ray diffractogram analysis. X-ray powder diffraction pattern of the sample was recorded from $2\theta = 10°$ to 90° on a Philips diffractometer Model PW 1710 using Cu Kα radiation at step 0.01° per second. The phase identification was performed using the search and match method by comparing the x-ray pattern of the sample to those of the standards in the JCPDF using Phase Identification from Powder Diffraction Files Window. The particle size was also determined using the Scherrer method [34].

Acid sites analysis. After heating at 90 °C, the sample was transferred into a crucible and placed in a vacuumed desiccator. Pyridine was transferred into another crucible and placed in the desiccator to allow the vapor of the pyridine to contact with the sample. After 24 h, the sample was taken from desiccator and left on open air for 2 h to expel the physically adsorbed pyridine from the sample.

Finally, the sample was analyzed using the FTIR spectroscopy. The analysis was conducted by grinding the sample with KBr of spectroscopy grade and scanned over the wave number in the range of 4000–400 cm^{-1} [35, 36].

TEM analysis. To evaluate the surface morphology, the samples were characterized using TEM. The analysis was conducted on polished and thermally etched samples with different magnifications [37].

Band-gap energy determination. To determine the band-gap energy of the $Ni_{0.5}V_{0.5}Fe_2O_4$ sample, a certain quantity of the sample was analyzed using UV-Vis Diffuse Reflectance Spectroscopy and scanned over the wavelength in the range of 200-800 nm [38].

Activity tests. About 300 mL of 10 ppm remazol golden yellow solution mixed with 100 mg of catalyst and stirred with a magnetic stirrer and then irradiated with sunlight at 12:00-13:00 with the time interval of 0, 20, 40, 60, 80, and 100 min. Furthermore, after the time interval was reached, 20 mL samples were taken to be analyzed by UV-Vis spectroscopy at a wavelength of 407 nm. Then, by interpolation of the absorbance of the sample to the absorbance of the standard curve of remazol golden yellow solution with known concentration, the degradation percentage of remazol golden yellow can be calculated.

Results and Discussion

X-ray Diffraction analysis. The X-ray diffraction analysis was carried out on the sample calcined at 600 °C and the diffraction pattern of $Ni_{0.5}V_{0.5}Fe_2O_4$ together with some standards related to the prediction phases of the sample was shown in Fig. 1a. With the aid of PCPDF-Win program, it was found that the major phases are spinels of $FeFe_2O_4$ (PDF-19-0629), $NiFe_2O_4$ (PDF-44-1485), FeV_2O_4 (PDF-15-0122). Additional phases identified are $NiVO_3$ (PDF-27-1308), V_3O_4 (PDF-34-0615), and NiO (PDF-47-1049) as the minor phases.

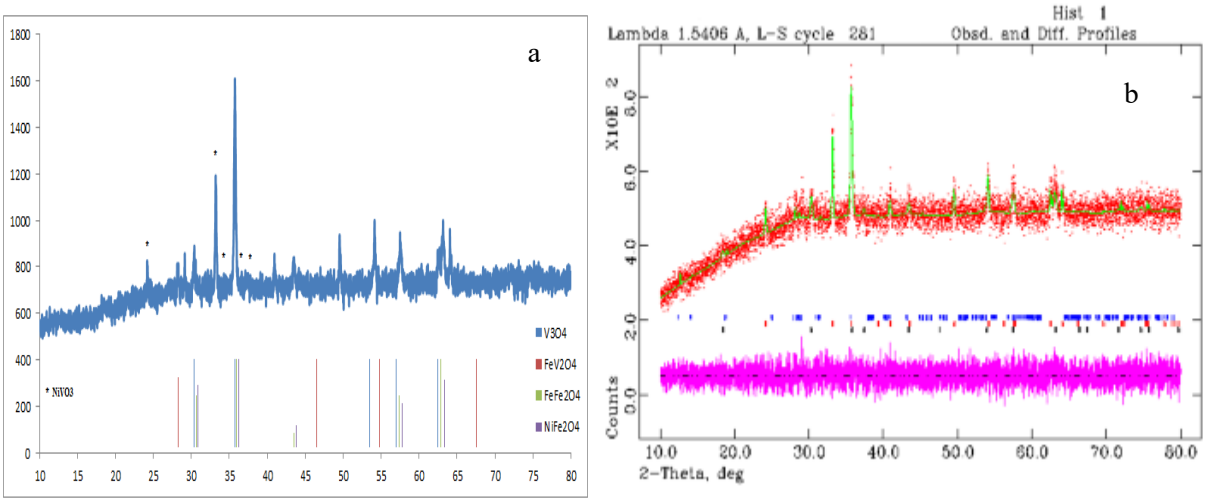

Figure 1. The diffraction pattern and rietveld analysis of $Ni_{0.5}V_{0.5}Fe_2O_4$

Since the diffraction pattern of some spinel is superimposed such as $NiFe_2O_4$, FeV_2O_4, and $FeFe_2O_4$, it can be inferred that there is a $Ni_{0.5}V_{0.5}Fe_2O_4$ structure. These normal and inverse spinels have a cubic structure (Fd3m SG). Furthermore, Rietveld analysis which is shown in Fig. 1b proved that there is cubic (normal and inverse spinel), and rhombohedral (Fe_2O_3 and V_3O_4) as the major phases too and monoclinic of V_2O_5 as a minor phase. The Rietveld analysis data is tabulated in Table 1 below.

Table 1. Rietveld analysis result of $Ni_{0.5}V_{0.5}Fe_2O_4$ ($\chi^2 = 1.127$ and Wrp = 4.92)

Compounds	Structure phases	Cell parameters			Volume ($Å^3$)	Fraction (%)
		a (Å)	b (Å)	c (Å)		
$NiFe_2O_4$	cubic	8.329	8.329	8.329	577.97	48.87
Fe_2O_3 and V_3O_4	hexagonal	5.0303	5.0303	13.740	301.1	44.41
V_2O_5	monoclinic	7.108	3.572	6.267	159.1	6.72

FTIR analysis. In this chance, Fourier Transform Infrared spectroscopy was used to identify the functional group exists in the sample, primarily to observe the existence of Lewis and BrØnsted-Lowry acid sites and the vibrations among Fe–O–Ni, Fe–O–V, and V–O–Ni bonds. The FTIR spectra of the sample investigated is presented in Fig. 2. As can be seen in Fig. 2, in the finger-print region, there is an absorption band representing a stretching vibration of Fe-O and bending vibration of Ni–O and V–O at 594.06 cm^{-1} implying the existence of Ni–O–Fe, Fe–O–V, and Ni–O–V bonds which confirms the formation of $Ni_{0.5}V_{0.5}Fe_2O_4$ structure as expected [39].

In the sample investigated, the existence of the Lewis acid site is shown by the absorption band located at 1651.66 cm^{-1} and that of Brønsted- Lowry at 1481.3 cm^{-1} [40]. By comparing the % absorbance of those acid sites, it can be inferred that Lewis acid site is more prominent than Brønsted-Lowry site.

Microstructure analysis. In principle, the surface characteristic plays important roles in the application of solid material in the process. For this reason, the sample investigated in this study was characterized using TEM technique [41] and XRD for crystallite size determination using Scherrer calculation [34].

Characterization of the samples using TEM produced the micrographs as presented in Figure 3. In general, there are several structural shapes identified such as cubic, hexagonal, and monoclinic which are following the result of X-ray diffraction analysis. If focusing on spinel structure as a major phase, it displays, the existence of $Ni_{0.5}V_{0.5}Fe_2O_4$ crystalline phase as a unit cell. However, in a certain area, the presence of a bigger spinel structure (darkness shapes) can be observed, which confirms the existence of agglomeration.

To predict the particle size, the Vernier Caliper apparatus was applied. According to this method, the grain size can be defined as the average of the size at five different spots. Using this method, it was found that the grain size of the sample calcined 600 °C is 19.8 nm. Then, the crystallite size was calculated using the Scherrer method as a comparison. The formula is

$$D = \frac{k\lambda}{\beta \cos\theta}$$

Where D is the crystallite size (nm), k is a constant with the value in the range of 0.9-1.0 (in this calculation, k = 0.90), λ is the X-ray wavelength used, in this case, Cu-K_α = 0.15406 nm, β is the broadening of diffraction line measured at half maximum intensity, $\frac{\pi}{180} xFWHM$ (in radian), and θ is the Bragg's angle in degree unit. From Scherrer calculation, it was found that crystallite sizes of $Ni_{0.5}V_{0.5}Fe_2O_4$ calcined at 600 °C was 34.06 nm.

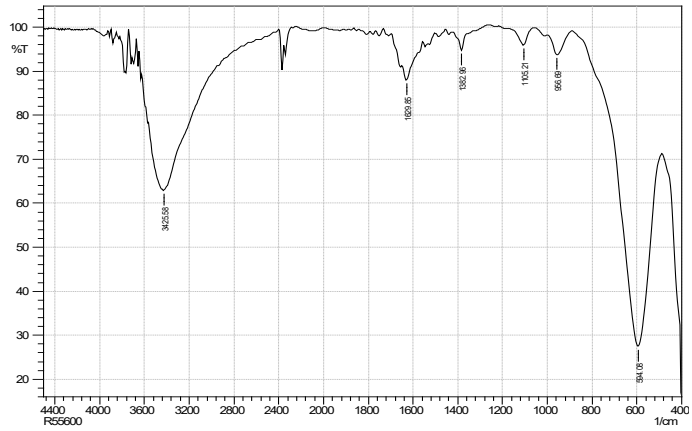

Figure 2. FTIR Spectra of $Ni_{0.5}V_{0.5}Fe_2O_4$ spinel after exposing to pyridine

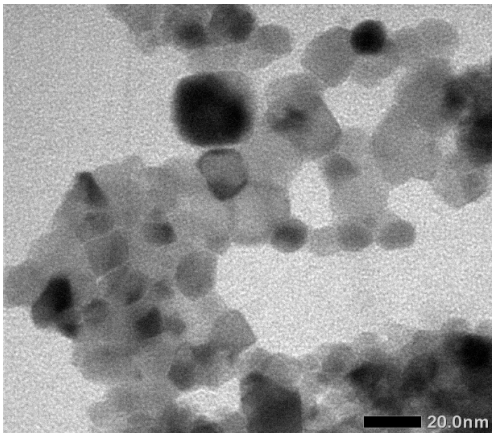

Figure 3. TEM micrograph of $Ni_{0.5}V_{0.5}Fe_2O_4$

Band-gap energy analysis. Data obtained from UV-Vis Diffuse Reflectance Spectroscopy was changed using the Kubelka-Munk formula [42] and Tauc plot [43]. Then, by making a graph

according to the equation $\{F(R)\ h\nu\}^n$ versus $(h\nu)$ and extrapolating to the X-axis until the value of Y-axis, $\{F(R)\ h\nu\}^2$ goes to zero, the bandgap energy was obtained as 2.0 eV. This value indicates that $Ni_{0.5}V_{0.5}Fe_2O_4$ nanomaterial can work in the visible irradiation region as a photocatalyst.

Photodegradation remazol golden yellow. In this experiment, remazol golden yellow was decomposed into molecules of H_2O, CO_2, NO_2, and SO_2 after photocatalysis under sunlight irradiation. The percentage of degradation that was produced on the contact time under sunlight irradiation increased and reached 45% as shown in Fig. 5 below.

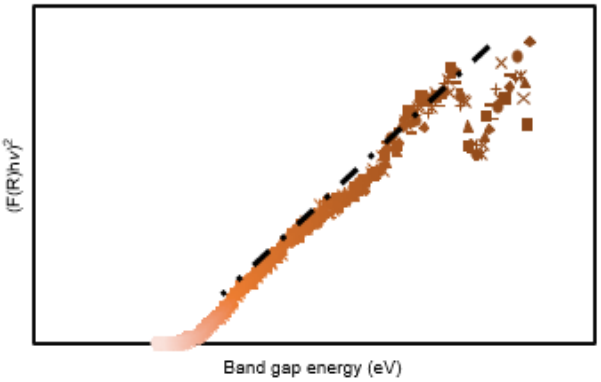

Figure 4. Bandgap energy of $Ni_{0.5}V_{0.5}Fe_2O_4$ calcined at 600 °C

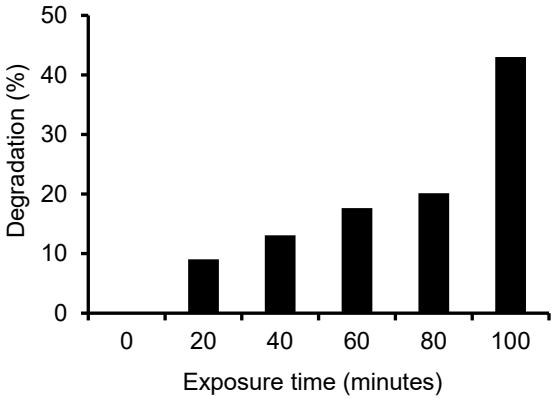

Figure 5. Remazol golden yellow photodegradation under sunlight irradiation

Furthermore, by assuming that the rate of photodegradation is a pseudo first-order or a second order through its kinetics equation and an indication of linearity, R-squared, which is 0.9695 and 0.9916, as shown in Fig. 6, respectively, it can be implied that this photocatalytic reaction occurred as a second-order reaction.

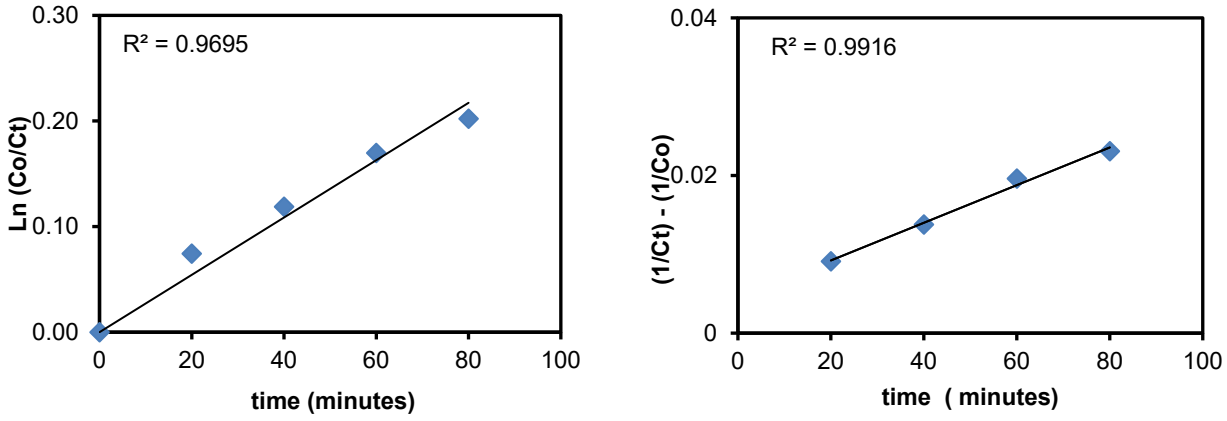

Figure 6. Linear regression of pseudo-first and second-order reaction on remazol golden yellow photodegradation under sunlight irradiation

Summary

This current study demonstrated the potential of pectin solution as a capping agent for preparing nano-size $Ni_{0.5}V_{0.5}Fe_2O_4$ material using the sol-gel method. The existence of nanoparticles in the sample was confirmed by the results of characterization techniques applied, including XRD and TEM, although particle agglomeration should also have existed. The sample was found to exhibit Lewis and Brønsted-Lowry acid characteristics, with Lewis acid as the dominant site, as revealed by the FTIR analyses. Furthermore, band-gap energy analysis indicated that the material can be work as a photocatalyst under visible light irradiation. This is proved that $Ni_{0.5}V_{0.5}Fe_2O_4$ nanomaterial was able to degrade remazol golden yellow in 45% conversion.

Acknowledgment

We thank the Minister of Research, Technology, and Higher Education of the Republic of Indonesia for providing research funding through the contract number 179/SP2H/LT/DRPM/2019.

References

[1] J. M. de Alvarenga, R. A. Fideles, M. V. de Silva, G. F. Murari, J. G. Taylor, L. R.de Lemos, G. D. Rodigues, A. B. Mageste, Partition study of textile dye remazol yellow gold RNL in aqueous two-phase systems, Fluid Phase Equilib. 391 (2015) 1-8.

[2] K. Santhi, P. Manikandan, C. Rani, S. Karuppuchamy, Synthesis of nanocrystalline titanium dioxide for photodegradation treatment of remazol brown dye, Appl. Nanosci. 5 (2015) 373-378.

[3] C. G. Maia, A. S. Oliveira, E. M. Saggioro, J. C. Moreira, Optimiztion of the photocatalytic degradation of commercial azo dyes in aqueuos TiO_2 suspensions, Reac. Kinet. Mech. Cat. 113 (2015) 305-320.

[4] J.K.D. de Souza, A.S.B. Silva, L.C. de Lima, E. Longo, A.G. de Souza, A. da Silva Maia, I. M. G. Santos, $NaNbO_3$ applied in the photodiscoloration of golden yellow remazol, XIV Brazil MRS Meeting-Rio de Janeiro, 2015.

[5] A.R. Phani, M. Passacantando, S. Santucci, Synthesis and characterization of zinc aluminum oxide thin films by sol-gel technique, Mater. Chem. Phys. 68 (2001) 66-71.

[6] M. Zawadzki, J. Wrzyszcz, W. Strek, D. Hreniak, Preparation and optical properties of nanocrystalline and nanoporous Tb doped alumina and zinc aluminate, J. Alloys Compd. 323-324 (2001) 279-282.

[7] C. Li, X. Han, F. Cheng, Y. Hu, C. Chen, J. Chen, Phase and composition controllable synthesis of cobalt manganese spinel nanoparticles towards efficient oxygen electrocatalysis, Nat. Commun. 6 (2015) 7345-7352.

[8] C. Baudin, R. Martinez, P. Pena, High-temperature mechanical behavior of stoichiometric magnesium spinel, J. Am. Ceram. Soc. 78 (1995) 1857-1862.

[9] T. D. Boyko, A. Hunt, A. Zerr, A. Moewes, Electronic structure of spinel-type nitride compounds Si_3N_4, Ge_3N_4, and Sn_3N_4 with tunable band gaps: application to light emitting diodes, Phys. Rev. Lett. 111 (2013) 0974021-0974025.

[10] Y. Wang, W. Tang, J. Cheng, M. Behtash, K. Yang, Creating two-dimensional electron gas in polar/polar perovskite oxide heterostructures: first-principles characterization of $LaAlO_3/A^{+}B^{5+}O_3$, ACS Appl. Mater. Interfaces 8 (2016) 13659-13668.

[11] M. Niyaifar, S. Nazari, H. Mohammadpour, Magnetic and structural studies of $Mg_{1-x}Zn_xFe_2O_4$. Proc. AES-ATEMA 18th Int. Conf., Canada, (2014). 203-212.

[12] K. M. Kojima, R. Kadono, M. Miyazaki, M. Hiraishi, I. Yamauchi, A. Koda, Y. Tsuchiya, H. S. Suzuki, H. Kitazawa, Magnetic frustration in iridium spinel compound $CuIr_2O_4$, Phys. Rev. Lett. 112 (2014) 087203.

[13] M. Doynov, T. Dimitrov, S. Kozhukharov, Alternative technological approach for synthesis of ceramic pigments by waste materials recycling, Boletín de la Sociedad Española de Cerámica y Vidrio 55 (2016) 63-70.

[14] Wendusu, T. Yoshida, T. Masui, N. Imanaka. Novel environmentally friendly inorganic red pigments based on calcium bismuth oxides, J. Adv. Ceram. 4 (2015) 39-45.

[15] X. Li, Z. Zhu, Q. Zhao, L. Wang, Photocatalytic degradation of gaseous toluene over $ZnAl_2O_4$ prepared by different methods: A comparative study, J. Hazard. Mater. 186 (2011) 2089-2096.

[16] S. Battiston, C. Rigo, E. da Cruz Severo, M. A. Mazutti, R. C. Kuhn, A. Gündel, E. L. Foletto, Synthesis of zinc aluminate ($ZnAl_2O_4$) spinel and its application as photocatalyst, Mat. Res. 17 (2015) 734-738.

[17] D. E. Zhang, X. J. Zhang, X. M. Ni, H. G. Zheng, D. D. Yang, Synthesis and characterization of $NiFe_2O_4$ magnetic nanorods via a PEG-assisted route, J. Magn. Magn. Mater. 292 (2005) 79-82.

[18] K. Sreekumar, S. Sugunan, Ferrospinels based on Co and Ni prepared via a low temperature route as efficient catalysts for the selective synthesis of o-cresol and 2,6-xylenol from phenol and methanol, J. Mol. Catal. A Chem. 185 (2002) 259-268.

[19] R. Situmeang, S. Wibowo, W. Simanjuntak, R. Supryanto, R. Amalia, M. Septanto, P. Manurung, S. Sembiring, Characteristics of nanosize spinel $NixFe_{3-x}O_4$ prepared by sol–gel method using egg white as emulsifying agent, Indones. J. Chem. 15 (2015) 116-122.

[20] C. R. Vestal, Z. J. Zhang, Effects of surface coordination chemistry on the magnetic properties of $MnFe_2O_4$ spinel ferrite nanoparticles, J. Am. Chem. Soc. 125 (2003) 9828-9833.

[21] J. G. S. Duque, E. A. Souza, C. T. Meneses, L. Kubota, Magnetic properties of $NiFe_2O_4$ nanoparticles produced by a new chemical method. Physica B Condens. Matter. 398 (2007) 287-290.

[22] P. Sivakumar, R. Ramesh, A. Ramanand, S. Ponnusamy, C. Muthamizhchelvan, Preparation of sheet like polycrystalline $NiFe_2O_4$ nanostructure with PVA matrices and their properties. Mater. Lett. 65 (2011) 1438-1440.

[23] R. J. Hill, J. R. Craig, G. V. Gibbs, Systematics of the spinel structure type, Phys. Chem. Miner. 4 (1979) 317-339.

[24] M. A. Ahmed, S. I. El-Dek, I. M. El-Kashef, N. Helmy, Structural and magnetic properties of nano-crystalline Ag^+ doped $NiFe_2O_4$, Solid State Sci. 13 (2011) 1176-1179.

[25] M. Srivastava, A. K. Ojha, S. Chaubey A. Materny, Synthesis and optical characterization of nanocrystalline $NiFe_2O_4$ structures, J. Alloys Compd. 481 (2009) 515-519.

[26] M. S. Niasari, F. Davar, T. Mahmoudi, A simple route to synthesize nanocrystalline nickel ferrite ($NiFe_2O_4$) in the presence of octanoic acid as a surfactant, Polyhedron 28 (2009) 1455-1458.

[27] P. Sivakmar, R. Ramesh, A. Ramanand, S. Ponnusamy, C. Muthamizhchelvan, Synthesis and characterization of $NiFe_2O_4$ nanosheet via polymer assisted co-precipitation method, Mater. Lett. 65 (2011) 483-485.

[28] A. Alarifi, N. M. Deraz, S. Shaban, Structural, morphological and magnetic properties of $NiFe_2O_4$ nano-particles, J. Alloys Compd. 486 (2009) 501-506.

[29] H. Li, H. Z. Wu, G. X. Xiao, Effects of synthetic conditions on particle size and magnetic properties of $NiFe_2O_4$, Powder Technol. 198 (2010) 157-166.

[30] N. A. El-Shafi, M. M. Morsi, Optical absorption and infrared studies of some silicate glasses containing titanium, J. Mater. Sci. 32 (1997) 5185-5189.

[31] S. Klosek, D. Raftery, Visible light driven V-doped TiO_2 photocatalyst and its photooxidation of ethanol, J. Phys. Chem. B 105 (2001) 2815-2819.

[32] V. Shanmugam, S. Sanjeevamuthu, K. S. Jeyaperumal, R. Vairamuthu, Fabrication of heterostructured vanadium modified γ-C_3N_4/TiO_2 hybrid performance under visible light exposure and antibacterial activities, J. Ind. Eng. Chem. 76 (2019) 318-332.

[33] K. S. Por, O. Y. Khai, S. L. Lee, Vanadium oxides doped poroustitania photocatalyst for phenol photodegradation, Malaysian Journal of Fundamental and Applied Sciences 1 (2016) 1-86

[34] B. D. Cullity, Elements of X-ray Diffraction, second ed., Addison-Wesley Publishing Company Inc., Phillipines, 1978.

[35] E. P. Parry, An infrared study of pyridine adsorbed on acidic solids. Characterization of surface acidity, J. Catal. 2 (1963) 371-379.

[36] J. Ryczkowski, IR spectroscopy in catalysis, Catal. Today 68 (2001) 263-381.

[37] D. V. Sridhara Rao, K. Muraleedharan, C. J. Humphreys, in A. Méndez-Vilas, J. Díaz (Eds.), Microscopy: Science, Technology, Applications and Education, Formatex, Spain, 2010.

[38] N. Sangiorgi, L. Aversa, R. Tatti, R. Verucchi, A. Sanson. Spectrophotometric method for optical band gap and electronic transitions determination of semiconductor materials. Opt. Mater. 64 (2017) 18-25.

[39] K. Tanabe, M. Misoono, H. Hattori, Y. Ono, New solid acids and bases, their catalytic properties, Kodansha Ltd., Tokyo-Japan, Academic Press, New York-London, 1990.

[40] M. Yurdakoç, M. Akçay, Y. Tonbul, K. Yurdakoç, Acidity of silica-alumina catalysts by amine titration using Hammett indicators and FT-IR study of pyridine adsorption. Turk. J. Chem. 23 (1999) 319-327.

[41] L. D. Hanke, Handbook of Analytical Method for Materials, Material Evaluation and Engineering Inc. Plymouth, America, 2001.

[42] N. Sangiorgi, L. Aversa, R. Tatti, R. Verucchi, A. Sanson, Spectrophotometric method for optical band gap and electronic transitions determination of semiconductor materials, Opt. Mater. 64 (2017) 18-25.

[43] J. Tauc, R. Grigorovici, A. Vancu, Optical properties and electronic structure of amorphous germanium, Phys. Status Solidi B 15 (1966) 627-637.